Dual-excitation multispectral fluorescence lifetime imaging handheld endoscope for label-free metabolic and biochemical imaging of the oral mucosa

GABRIEL TORTORELLI,[1] RODRIGO CUENCA,[1] MICHAEL J. SERAFINO,[1] KAYLA CAUGHLIN,[2] CARLOS BUSSO,[2] VICTORIA L. WOO,[3] JACQUELINE PLEMONS,[3] YI-SHING L. CHENG,[3] CELESTE ABRAHAM,[3] YING S. WANG, RASHMI HEGDE,[3] JAVIER A. JO[1,*]

[1]*School of Electrical and Computer Engineering, University of Oklahoma, Norman, OK 73019 USA*
[2]*Department of Electrical and Computer Engineering, University of Texas, Dallas Richardson, TX 78712 USA*
[3]*Department of Diagnostic Sciences, Texas A&M University, Dallas, TX 75246 USA*
*javierjo@ou.edu

Received XX Month XXXX; revised XX Month, XXXX; accepted XX Month XXXX; posted XX Month XXXX (Doc. ID XXXXX); published XX Month XXXX

This work introduces a dual-excitation, multispectral-detection, frequency-domain fluorescence lifetime imaging (FLIM) handheld endoscopy system for comprehensive autofluorescence imaging of the oral mucosa. The excitation wavelengths and spectral detection channels were selected to preferentially image the fluorescence of endogenous fluorophores relevant for oral epithelial cancer detection. The endoscope dimensions and optical specifications enable direct imaging of oral lesions with minimal patient discomfort. Comprehensive imaging experiments using standard fluorophores demonstrate the capabilities of the FLIM endoscope to measure a wide range of fluorescence lifetimes (0.1-12 ns) with high precision (~100 ps). Clinical *in vivo* label-free metabolic and biochemical endoscopic FLIM imaging was demonstrated by imaging a malignant oral lesion and healthy mucosa in a patient undergoing a tissue biopsy procedure.

http://doi.org/10.xxxxxxxxxxxxxxxxxxxxxxxxxxxx

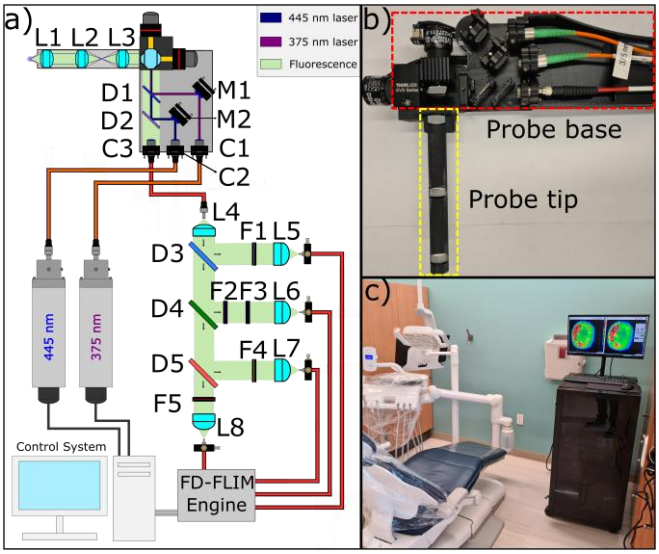

Fig. 1. (a) Schematic of the dual-excitation multispectral FD-FLIM endoscopy system. (b) Photograph of the handheld endoscopic probe. (c) Photograph of the FD-FLIM endoscopy system installed in a dental office at the Texas A&M College of Dentistry, Dallas, TX.

Introduction. The incidence of oral cancer has been increasing over the last 20 years, with over 58,000 new cases expected annually, according to the American Cancer Society (ACS) [1]. When diagnosed at early stages, the 5-year survival rate is 87%. However, when diagnosed at intermediate or advanced stages, the 5-year survival rate drops to 69% and 39%, respectively. Unfortunately, benign oral lesions are often difficult to distinguish from dysplasia or early-stage cancer. As a result, only about 30% of patients are diagnosed at early stages despite the fact that the oral cavity is easily accessible for direct examination. Hence, there is a critical need for new clinical technologies that will facilitate reliable early diagnosis of oral cancer and dysplasia.

There are several morphological, biochemical, and functional biomarkers of oral dysplasia and cancer that modulate tissue autofluorescence [2]. Both epithelial thickening and collagen degradation occur in dysplasia and cancer, resulting in a decreased contribution of collagen to tissue autofluorescence. Increased metabolic activity, a hallmark of epithelial cell malignant transformation, induces subtle changes in oral tissue autofluorescence originating from mitochondrial flavin adenine dinucleotide (FAD) and the reduced form of nicotinamide adenine dinucleotide (NADH), which are highly specific to oral dysplasia and cancer. Additionally, endogenous protoporphyrin IX (PpIX) has been observed in dysplastic and malignant oral lesions [3]. Our group has been establishing the potential of endogenous fluorescence lifetime imaging (FLIM) endoscopy as a clinical tool to facilitate the early detection of oral cancer [4-7]. In this Letter, we describe a novel dual-excitation multispectral FLIM endoscopy system specifically designed for label-free metabolic and biochemical imaging of the oral mucosa (**Fig. 1**).

Imaging system design. The endoscopy system was developed based on a versatile, practical, and cost-effective frequency-domain (FD) FLIM design recently introduced by our group [8]. Simultaneous fluorescence excitation at 375 nm and 445 nm is achieved using frequency-multiplexed digital pulse modulation of continuous-wave (CW) diode lasers (Toptica iBeam-Smart-375 and iBeam-Smart-445). Time-resolved fluorescence detection across four emission spectral bands is implemented using fixed-gain avalanche photodiodes (APD) (Hamamatsu C12702-11). The FD-FLIM engine, implemented using a common field-programmable gate array (FPGA) available in a development board (Xilinx ZedBoard Zynq-7000), provided synchronized laser modulation and fluorescence signal digitization. Simultaneous multispectral time-resolved fluorescence signal digitalization is performed at 250 MHz sampling rate using a 4-channel ADC FPGA-mezzanine-card (Abaco FMC104). The use of the FPGA also permits real-time calculation of both the magnitude and phase frequency response of the fluorescence emission across multiple modulation frequencies and emission spectral channels. Dual-excitation multispectral FD-FLIM imaging and real-time frequency response calculation is performed at a pixel rate of 12.5 kHz.

To deliver the excitation light into the handheld endoscope probe (**Fig. 1(a)**), each laser output is coupled into 3-meter multimode fibers (NA = 0.22, d = 50 µm, Thorlabs FG50UGA). In the handheld probe base, each laser excitation beam is collimated (C1-C2, Thorlabs F671FC-405) and combined into a common optical path by a series of reflective (M1-M2: Thorlabs BB05-E01) and dichroic (D1: Chroma T387lp; D2: Chroma ZT442dcrb-UF1) mirrors. The common optical path is aligned with the center of the lower of two galvanometric mirrors (Thorlabs GVS202) used for simultaneous scanning of the two excitation beams onto the sample through a rigid endoscope built using three achromatic double lenses (L1-L3). The sample fluorescence emission is collected through the same lenses (L1-L3), de-scanned by the galvanometric mirror set, and coupled (C3, Thorlabs F220-SMA) into a 3-meter multimode fiber (NA = 0.22, d = 600 µm, Thorlabs FG600AEA).

A photograph of the handheld endoscopic probe is shown in **Fig. 1(b)**. The 3D-printed probe base (**Fig. 1(b)**, red dashed box) is 71 mm in width and 210 mm in length and has holders for mounting the galvanometric mirrors, the rigid endoscope, and the alignment optics. The base was designed so that the height of the collimators and reflective/dichroic mirrors can be adjusted to match the optical center height of the lower galvanometric mirror. To facilitate the alignment of the optical paths for both the excitation beams and fluorescence emission, kinematic mounts (Thorlabs MK05 and MK11F) were used to position both the mirrors M1-M2 and the collimators C1-C3. The three optical fibers are fixed to the base to reduce the tension force on the collimators.

Oral epithelial lesions are typically smaller than 10 mm in length/width and can be found at any location inside the oral cavity. To reach most oral lesions without inducing major discomfort to the patient, a rigid endoscope was designed with a field of view (FOV) of ~78 mm² (circular FOV, ~10 mm in diameter), lateral resolution of ~250 µm, length >100 mm, and diameter <15 mm. Simulations were conducted in Zemax to determine components for a rigid endoscope with these specifications. A simple system with three achromatic lenses (L1-L3, f = 25 mm, d = 12.5 mm, Edmund Optics 65-971), where L1 works as an objective and L2-L3 serve as an image relay, was found to meet these requirements. The 3D-printed rigid endoscope consists of a lens tube (length: 123 mm; outer diameter: 13.5 mm) with slits for pressure holding the three lenses L1-L3 (**Fig. 1(b)**, yellow dashed box). Lens L3 is placed at a distance to the midpoint between the two galvanometric mirrors equal to its focal length. Lens L2 is placed to form a telescopic system alongside lens L3, while Lens L1 is placed at the focal point of L2.

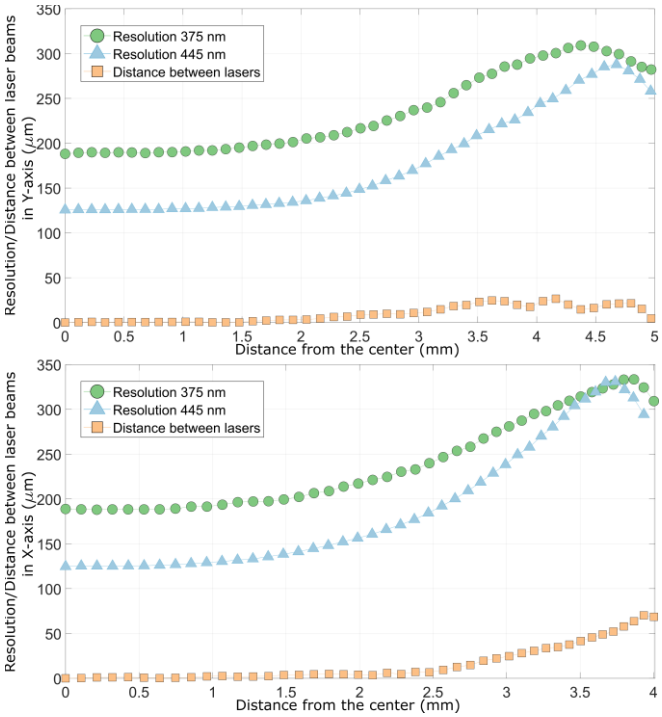

Fig. 2. Optical resolution, scan range, and co-alignment of the two excitation beams measured in both scanning axes. Resolution was measured as the 1/e² beam diameter. Co-alignment was measured as the distance between the two excitation beams. The scan range in the Y-axis is larger than in the X-axis.

The fluorescence emission is transmitted through the collection fiber to an optical cage system, where the emission is collimated (L4, f = 40 mm, d = 1 inch, Thorlabs LA1422-A) and separated into four spectral channels through a series of dichroic mirrors (D3: Chroma AT440dc; D4: Semrock FF506-Di03; D5: FF01-647/57-25) and optical filters (F1: Chroma ET405|40x; F2: Chroma AT465lp; F3: Semrock FF02-475/50-25; F4: Semrock FF01-550/88-25; F5: Semrock FF01-647/57-25). The resulting emission spectral channels were customized to preferentially image the oral mucosa autofluorescence originating from collagen (405±20 nm), NADH (482±18 nm), FAD (550±44 nm), and PpIX (647±28 nm). The output of each spectral channel is coupled (L5-L8, f = 25 mm, d = 1 inch, Thorlabs LA1951-A) into a multimode fiber (NA = 0.50, d = 600 µm, Thorlabs FP600ERT) to transmit the emission light onto the active area of an APD installed inside an RF-shielded enclosure.

Imaging system optical specifications. The optical resolution, scan range, and co-alignment of the two excitation beams were measured as follows. The galvanometric mirrors were centered at the middle of the sensor of a CMOS camera (Allied Vision Manta G-419) mounted at the focal plane of L1. The voltage of each scanning mirror was varied independently, until the maximum scan angle (12.5°) was reached. At each voltage value, the resolution (1/e² beam diameter) and the distance to the center of each laser beam were imaged and measured for each axis, as shown in **Fig. 2**.

For both excitation wavelengths, the resolution was fairly constant at the middle of the scan range (<200 µm for 375 nm; <150 µm for 445 nm), before starting to increase with the distance to the center due to spherical aberration introduced by the lenses. Overall, the resolution was <300 µm for the two excitation wavelengths in both axes. There is a notable difference in the scan range between the two axes, due to the difference in distance between each scanning mirror and the first lens (L3) of the relay system, with the Y-axis (closer mirror) scanning larger angles before clipping compared to the X-axis (farther mirror). The resulting FOV has an elliptical shape (semi-minor axis: 4 mm; semi-major axis: 5 mm) with an area of ~63 mm². The distance between the two excitation beams was <50 µm for the entire range of the Y-scan and for most of the range of the X-scan, and less than 1/5 of the optical resolution of any of the excitations at any beam position, demonstrating co-alignment of the two excitation beams in the entire FOV.

Imaging speed and excitation power. All FLIM images were acquired at a pixel rate of 12.5 kHz, 160x160 pixels per image (acquisition time: ~2 s per image), and average powers of 11 mW and 17 mW at the sample for the 375 nm and 445 nm excitations, respectively. To ensure safe *in vivo* imaging of the oral mucosa, the maximum permissible exposure (MPE) was calculated following guidelines provided by the American National Standards Institute (ANSI) for Safe Use of Lasers [9]. Accordingly, the MPE for each excitation was calculated based on a 3.5 mm limiting aperture. The number of pixels in a 3.5 mm aperture is $N_{3.5\emptyset}$= [π(3.5mm/2)^2]/ [10mm/160px * 8mm/160px] = 3079 pixels. The exposure time to scan a 3.5 mm aperture is given by is $T_{3.5\emptyset} = N_{3.5\emptyset}/12.5kHz = 0.2463$ seconds. For the 375 nm excitation, the exposure is Exp_{375nm} = (11mW)*$T_{3.5\emptyset}$/[π (3.5mm/2)^2]/10 = 0.02816 J.cm^{-2}, while the lower MPE corresponding to thermal effects is $MPE_{375nm} = 0.56*T_{3.5\emptyset}^{0.25}$ = 0.39 J.cm^{-2}. For the 445 nm excitation, the exposure is Exp_{445nm} = (17mW) * $T_{3.5\emptyset}$/ [π (3.5mm/2)^2]/ 10 = 0.0435 J.cm^{-2}, while the lower MPE corresponding to thermal effects is $MPE_{445nm} = 1.1* T_{3.5\emptyset}^{0.25}$ = 0.77 J.cm^{-2}. Thus, the used imaging parameters warranty excitation exposure levels of at least one order of magnitude lower than the corresponding MPE levels for both excitation wavelengths.

Validation with fluorescence standards. To quantify the precision of the dual-excitation multispectral FLIM endoscopy system to measure fluorescence lifetimes, a set of twelve fluorescence standard solutions were imaged: POPOP, NADH, Anthracene, DPA, Coumarin-1, 9CA, Rhodamine B, Rose Bengal, Fluorescein, FAD, Coumarin-6, and Rubrene (solvent and concentration for each fluorophore solution is provided in the Supplemental Document: **Table S1**). Each fluorophore solution was loaded in a quartz cuvette and imaged with the handheld FLIM endoscope. From the fluorophore FD-FLIM data, the fluorescence average lifetime ($\tau_{AVG-FDFLIM}$) was calculated using a non-linear least-square curve fitting method [10]. The fluorescence average lifetime ($\tau_{AVG-TCSPC}$) of each fluorophore solution was also measured using a calibrated Time-Correlated-Sigle-Photon-Counting (TCSPC) spectrometer DeltaPro-DD (Horiba, Japan) using the same excitation wavelengths and emission spectral channels as in the handheld endoscopy system. The average lifetimes measured upon specific excitations (λex) at specific emission spectral channels (λem) for each fluorophore solutions are summarized in **Table 1**. Good agreement between the average lifetimes measured with the two instruments was verified by means of correlation and Bland-Altman plots (Supplemental Document: **Fig. S1** and **Fig. S2**).

Table 1. Measured average lifetimes of fluorescence standards.

Fluorophore	λ_{ex} (nm)	λ_{em} (nm)	$\tau_{avg-TCSPC}$ (ns)	$\tau_{avg-FDFLIM}$ (ns)
POPOP	375	405 ± 20	1.289	1.274 ± 0.009
		482 ± 18	1.289	1.282 ± 0.014
		550 ± 44	1.294	1.299 ± 0.031
NADH	375	482 ± 18	0.499	0.520 ± 0.011
		550 ± 44	0.494	0.482 ± 0.009
ANT	375	405 ± 20	4.137	4.102 ± 0.059
DPA	375	405 ± 20	6.123	6.180 ± 0.063
Coumarin-1	375	405 ± 20	3.149	3.065 ± 0.068
		482 ± 18	3.207	3.314 ± 0.022
		550 ± 44	3.217	3.252 ± 0.040
9CA	375	482 ± 18	12.014	12.542 ± 0.121
		550 ± 44	11.932	12.386 ± 0.148
Rhodamine B	375	550 ± 44	1.616	1.574 ± 0.032
	445		1.547	1.569 ± 0.063
Rose Bengal	375	647 ± 28	0.102	0.109 ± 0.072
	445		0.092	0.098 ± 0.007
Fluorescein	445	482 ± 18	3.857	3.956 ± 0.089
		550 ± 44	3.944	3.937 ± 0.047
FAD	445	550 ± 44	2.959	3.399 ± 0.093
		647 ± 28	3.560	3.564 ± 0.048
Coumarin-6	445	482 ± 18	2.442	2.468 ± 0.009
		550 ± 44	2.457	2.499 ± 0.019
Rubrene	445	550 ± 44	7.433	7.473 ± 0.049
		647 ± 28	7.446	7.512 ± 0.094

In vivo imaging of oral lesion. The dual-excitation multispectral FLIM endoscopy system was installed at the Texas A&M College of Dentistry (**Fig. 1(c)).** Following an imaging protocol approved by the Institutional Review Board, a patient with an oral lesion in the left mandibular gingiva was imaged with the FLIM endoscope. An additional FLIM endoscopy image was acquired from a healthy-looking area on the contralateral side of the lesion. After FLIM imaging, a tissue biopsy was taken from the center of the oral lesion. The histopathological diagnosis indicated well to moderately differentiated squamous cell carcinoma (SCC).

The normalized multispectral fluorescence intensity maps indicate the fraction of the emission fluorescence detected at each emission spectral channel (λem) upon a specific excitation (λex): $I_{n,\lambda ex,\lambda em}(x,y) = \frac{I_{\lambda ex,\lambda em}(x,y)}{\Sigma_{\lambda em} I_{\lambda ex,\lambda em}(x,y)}$, where $I_{\lambda ex,\lambda em}(x,y)$ is the map of the absolute fluorescence intensity of emission spectral channel λem upon excitation λex, and the sum is over all the emission spectral channels. The absolute multispectral fluorescence intensity maps were also used to calculate the Redox Ratio map reflecting the relative contribution of FAD ($I_{445,554}(x,y)$) and NADH ($I_{337,484}(x,y)$) to the tissue autofluorescence: $REDOX(x,y) = \frac{I_{445,554}(x,y)}{I_{445,554}(x,y)+I_{337,484}(x,y)}$. In the FLIM endoscopy FOV of the healthy contralateral side, these maps were spatially homogenous (**Fig. 3**, top). Stronger fluorescence was observed at the 482±18 nm channel upon 375 nm excitation (associated with NADH contribution) and at the 550±44 nm channel upon 445 nm excitation (associated with FAD contribution). The REDOX map was also spatially homogeneous with values ~0.5. In the FLIM endoscopy FOV of the malignant gingiva oral lesion, all maps were spatially heterogenous, as the FOV includes the oral

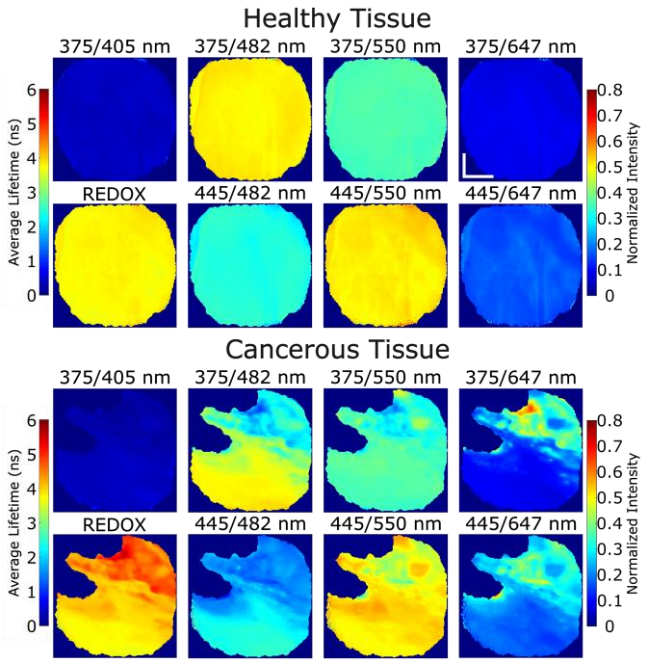

Fig. 3. Normalized multispectral fluorescence intensity maps for each combination of excitation and spectral emission channel (λex/λem) and REDOX maps for healthy contralateral mucosa (top) and malignant gingiva oral lesion (Bottom). Scale bar: 2 mm.

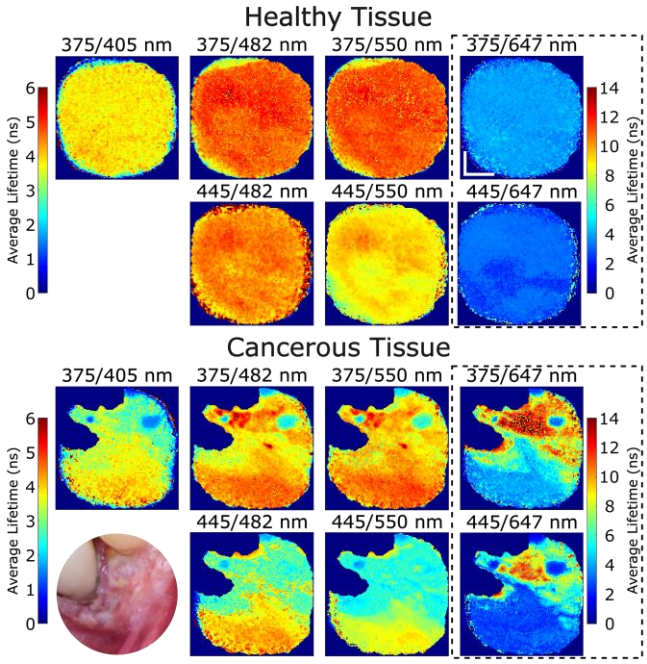

Fig. 4. Fluorescence average lifetime maps for each λex/λem for healthy contralateral mucosa (top) and malignant gingiva oral lesion (Bottom). A photograph of the gingival malignant lesion is shown for anatomical reference. Scale bar: 2 mm.

lesion around the masked teeth and surrounding healthy mucosa at the bottom of the FOV (**Fig. 3**, bottom). The region at the bottom of the FOV showed similar normalized fluorescence intensity and REDOX values as in the contralateral healthy side. The region corresponding to the gingival lesion (for spatial context, see oral lesion photograph in **Fig. 4**) showed weaker emission at both the 482±18 nm and 550±44 nm channels and stronger emission at the 647±28 nm channel for both excitations, the later associated to increased PpIX fluorescence contribution. The reduction in the emission at the 482±18 nm channel upon 375 nm excitation was more significant (lower NADH contribution), resulting on higher REDOX values in the malignant oral lesion, suggesting increased cellular metabolism through oxidative phosphorylation.

The corresponding fluorescence average lifetime maps $\tau_{avg,\lambda ex,\lambda em}(x,y)$ for each emission spectral channel upon a specific excitation are shown in **Fig. 4** (notice wider lifetime range for the 647±28 nm channel maps). In the FLIM endoscopy FOV of the healthy contralateral side, these maps were spatially homogenous (**Fig. 4**, top), while for the malignant gingiva oral lesion, all maps were spatially heterogenous (**Fig. 4**, bottom). The region at the bottom of the FOV showed similar fluorescence average lifetime values in all maps as in the healthy side. The region corresponding to the gingival lesion (for spatial context, see oral lesion photograph in **Fig. 4**) showed much longer average lifetime values (>8 ns) at the 647±28 nm channel, another indication of increased PpIX fluorescence contribution. The gingiva lesion region also showed shorter average lifetime values at the 550±44 nm channel upon 445 nm excitation, suggesting quenching of FAD, another indication of increased cellular metabolism through oxidative phosphorylation.

Discussion and conclusion. A dual-excitation, multispectral-detection FLIM handheld endoscopy system has been successfully developed for comprehensive autofluorescence imaging of the oral mucosa. The capabilities of this novel endoscopic tool to measure a wide range of fluorescence average lifetimes with high precision, and to enable label-free metabolic and biochemical endoscopic imaging of the oral mucosa, were rigorously demonstrated. Ongoing research is focused on evaluating the potential of dual-excitation, multispectral-detection FLIM endoscopy for the early detection of oral cancer in a multicenter clinical study.

Funding. National Institute of Health (R01CA218739, P20GM135009).

Disclosures. The authors declare no conflict of interest.

Data availability. Data underlying the results presented in this Letter are not publicly available but may be obtained upon reasonable request.

Supplemental Document. See Supplement 1 for supporting content.

REFERENCES

1. A. C. Society, *Cancer facts & figures 2024* (American Cancer Society, 2024).
2. I. Pavlova, M. Williams, A. El-Naggar et al., Clinical Cancer Research **14**, 2396-2404 (2008).
3. H. M. Chen, C. P. Chiang, C. You et al., Lasers in Surgery and Medicine: The Official Journal of the American Society for Laser Medicine and Surgery **37**, 37-45 (2005).
4. K. Caughlin, E. Duran-Sierra, S. Cheng et al., IEEE journal of biomedical and health informatics **27**, 457-468 (2022).
5. K. Caughlin, E. Duran-Sierra, S. Cheng et al., Cancers **16**, 4120 (2024).
6. S. Cheng, R. M. Cuenca, B. Liu et al., Biomedical optics express **5**, 921-931 (2014).
7. E. Duran-Sierra, S. Cheng, R. Cuenca et al., Biomedical Optics Express **13**, 3685-3698 (2022).
8. M. J. Serafino, and J. A. Jo, Biomedical Optics Express **14**, 1608-1625 (2023).
9. A. N. S. Institute, *American national standard for safe use of lasers* (Laser Institute of America, 2007).
10. J. C. Lagarias, J. A. Reeds, M. H. Wright et al., SIAM Journal on optimization **9**, 112-147 (1998).